CLIMATE SCIENCE

10.1126/sciadv.1501130

Ocean acidification causes structural deformities in juvenile coral skeletons

Taryn Foster,[1,2,3]* James L. Falter,[1,2,3] Malcolm T. McCulloch,[1,2,3] Peta L. Clode[2,4]

Rising atmospheric CO_2 is causing the oceans to both warm and acidify, which could reduce the calcification rates of corals globally. Successful coral recruitment and high rates of juvenile calcification are critical to the replenishment and ultimate viability of coral reef ecosystems. Although elevated P_{CO_2} (partial pressure of CO_2) has been shown to reduce the skeletal weight of coral recruits, the structural changes caused by acidification during initial skeletal deposition are unknown. We show, using high-resolution three-dimensional x-ray microscopy, that ocean acidification (P_{CO_2} ~900 µatm, pH ~7.7) not only causes reduced overall mineral deposition but also a deformed and porous skeletal structure in newly settled coral recruits. In contrast, elevated temperature (+3°C) had little effect on skeletal formation except to partially mitigate the effects of elevated P_{CO_2}. The striking structural deformities we observed show that new recruits are at significant risk, being unable to effectively build their skeletons in the P_{CO_2} conditions predicted to occur for open ocean surface waters under a "business-as-usual" emissions scenario [RCP (representative concentration pathway) 8.5] by the year 2100.

INTRODUCTION

Atmospheric CO_2 is set to rise to >900 parts per million (ppm) by the end of the century under a "business-as-usual" scenario [RCP (representative concentration pathway) 8.5], with corresponding elevations in both oceanic temperature (+~3°C) and partial pressure of CO_2 (P_{CO_2}) (+~500 µatm) (*1*). Both ocean temperature and P_{CO_2} are key environmental factors affecting coral calcification rates (*2*–*4*). There is usually a parabolic relationship between temperature and calcification, with optimal temperatures for calcification normally defined by local conditions (*5*, *6*), and a negative correlation between calcification and P_{CO_2} (*7*, *8*). However, the interactive effect of elevated temperature and P_{CO_2} on calcification appears to be variable, with both positive (*9*–*11*) and negative (*2*, *11*, *12*) interactions reported in adult corals. Adult coral calcification is already thought to have declined by 14 to 30% worldwide in recent years, with some studies suggesting that elevated temperature and ocean acidification are the major causes (*3*, *4*).

Corals in their early life stages have also been shown to be sensitive to changes in temperature and P_{CO_2} (*13*–*18*). Successful reproduction and post-recruitment processes (particularly growth) are essential to maintaining coral reef health (*19*). Therefore, it is particularly important to know how these environmental changes will affect skeletal growth in the early stages of development, when tiny recruits (~1 mm) are most vulnerable to mechanical damage, overgrowth, and predation. Experiments examining the impact of ocean acidification on calcification of newly settled recruits have reported strong effects, with 20 to 60% reductions in skeletal mass under acidified conditions (*20*–*23*). However, the combined effect of elevated temperature and P_{CO_2} on skeletal mass may be dependent on geographical location, with a negative impact in the tropics (*24*) and a positive impact in the subtropics (*23*). These studies have highlighted the vulnerability of new recruits to ocean acidification and, in particular, their limited ability to calcify under high P_{CO_2} conditions. However, to date, such research has relied solely on bulk measurements of skeletal mass to assess these impacts. There have been no analyses of specific structural changes in the juvenile skeleton under acidification or warming.

Here, we used high-resolution three-dimensional (3D) x-ray microscopy and scanning electron microscopy (SEM) to examine the skeletons of newly settled coral recruits of an abundant plate coral species (*Acropora spicifera*) from the subtropical Houtman Abrolhos Islands in Western Australia. Recruits were grown for 1 month under four temperature-P_{CO_2} regimes: (i) control (24°C and 250 µatm, pH 8.2), (ii) elevated temperature ("high *T*"; 27°C and 250 µatm, pH 8.2), (iii) elevated P_{CO_2} ("high P_{CO_2}"; 24°C and 900 µatm, pH 7.7), and (iv) elevated temperature and elevated P_{CO_2} ("high T + P_{CO_2}"; 27°C and 900 µatm, pH 7.7) (see also table S1 and figs. S1 and S2). X-ray microscopy was used to generate 3D images and data of the skeletons to discern both visual and quantitative differences in skeletal structure between the four regimes. The 3D reconstructions enabled the extraction of bulk measurements (surface area and volume), cross-sectional measurements (height and basal plate thickness), and internal measurements (corallite wall thickness and tertiary septa width)—structural information that would be impossible to obtain using conventional 2D imaging methods (figs. S3 and S4). SEM images of the same individuals were also acquired to more closely examine abnormalities in the skeletal microstructure.

RESULTS

Coral skeletons from low P_{CO_2} treatments (control and high *T*) were typically radially symmetric and had six tertiary septa of similar size (Fig. 1, A and E, figs. S5 and S6, and movie S1). Skeletal surfaces of the low-P_{CO_2} corals were also smooth and appeared solid at both the corallite wall and tertiary septa (Fig. 1, C, D, G, and H; see also fig. S3 for the exact location of these structures on the coral skeleton). In contrast, high-P_{CO_2} corals had a variety of deformities disrupting their symmetry. Most high-P_{CO_2} corals had missing or unevenly sized tertiary septa, with recruits commonly having overgrown septa on one side of the mouth and missing or stunted septa on the other side

[1]UWA School of Earth and Environment, University of Western Australia, Crawley, Western Australia 6009, Australia. [2]UWA Oceans Institute, University of Western Australia, Crawley, Western Australia 6009, Australia. [3]ARC Centre of Excellence for Coral Reef Studies, University of Western Australia, Crawley, Western Australia 6009, Australia. [4]Centre for Microscopy, Characterisation and Analysis, University of Western Australia, Crawley, Western Australia 6009, Australia.
*Corresponding author. E-mail: taryn.foster@research.uwa.edu.au

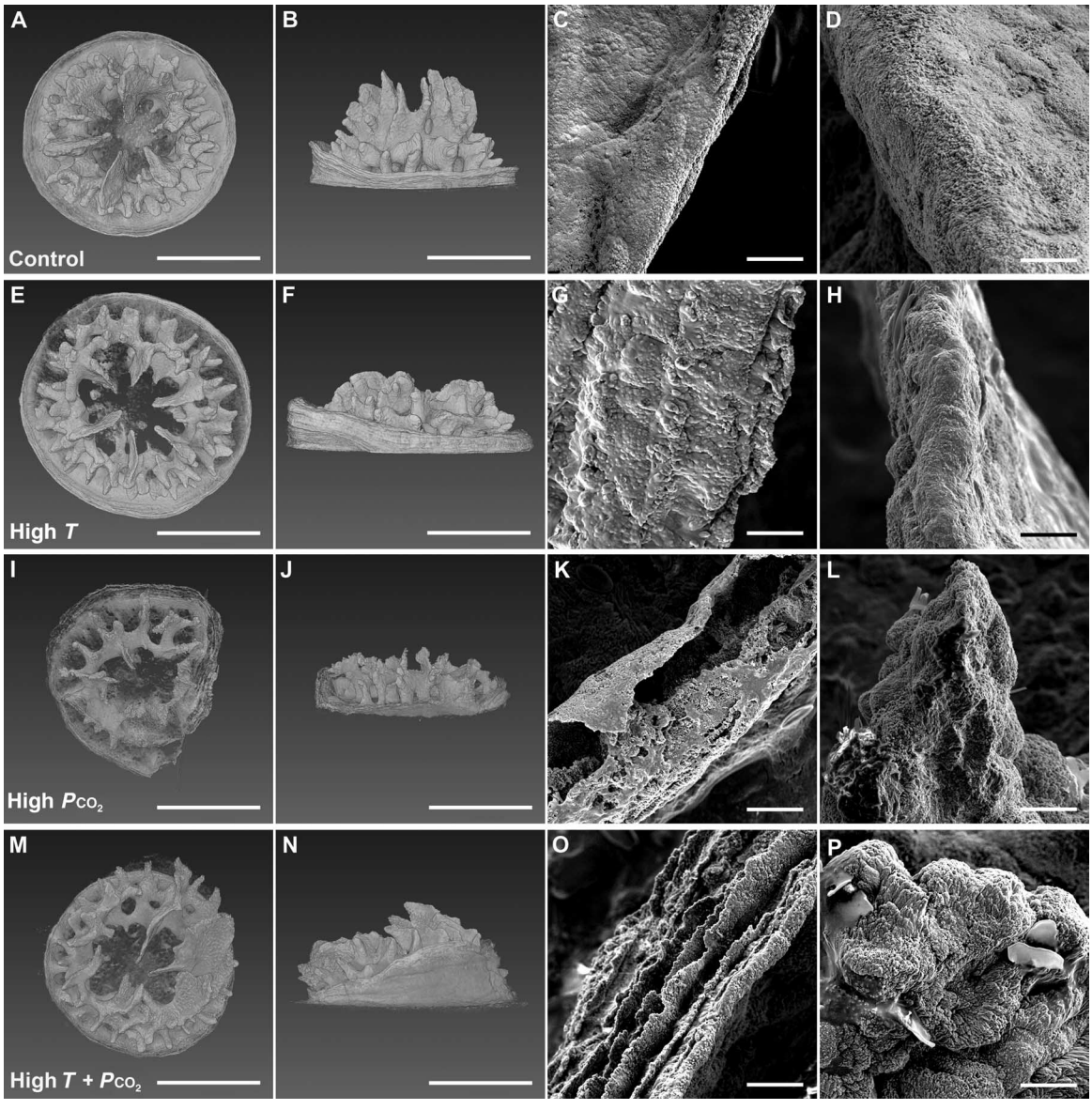

Fig. 1. X-ray microscopy and SEM images of 1-month-old coral skeletons under the four temperature-P_{CO_2} treatments (A to P). Treatments include control (A to D), high *T* (E to H), high P_{CO_2} (I to L), and high *T* + P_{CO_2} (M to P). 3D x-ray images: top-down view (A, E, I, and M) and side view (B, F, J, and N). Scale bars, 500 μm. SEM images: top of the corallite wall (C, G, K, and O) and a tertiary septum (D, H, L, and P). Scale bars, 10 μm. The four images shown in each row are of a single, representative individual from each treatment. See figs. S5 to S8 for images of the other individuals from each treatment.

(Fig. 1, I and M). Perhaps the most striking difference between high- and low-P_{CO_2} corals was the deep pitting and porous microstructure of the corallite wall (Fig. 1, K and O), a feature that was consistent across all individuals grown under high P_{CO_2} (figs. S7 and S8). Although not as severe, shallow pitting was also observed in the tertiary septa of the high-P_{CO_2} corals (Fig. 1, L and P, and figs. S7 and S8). Other deformities observed only in high-P_{CO_2} corals included small gaps in the lattice-like structure of septa and synapticulae (horizontal connecting structures) (Fig. 2, E and F) as well as more severe deformities, such as large sections of the skeleton being completely absent (Fig. 2, G and H, and movie S2). Fractures were also observed in the septa and corallite walls of 50% of the high-P_{CO_2} corals (Fig. 2, A to D), whereas no fractures were recorded in the low-P_{CO_2} corals.

High P_{CO_2} also significantly contributed to reductions in overall skeletal deposition, as shown by high surface area–to–volume ratios (SA/vol) as well as reduced diameter and basal plate thickness in high-P_{CO_2} corals under both temperature regimes (Fig. 3 and table S2). Furthermore, the length-to-width ratios of the tertiary septa were highly reduced because of malformation (that is, incomplete extension of the septa) in the high P_{CO_2} treatment, and vertical growth (height) was similarly stunted. Temperature alone appeared to have little effect, only significantly increasing tertiary septa length-to-width ratios. Post hoc comparisons showed that where there were statistically significant interactions between temperature and P_{CO_2} they were positive, with elevated temperature significantly increasing both height and tertiary septa length-to-width ratios under high P_{CO_2} ($P = 0.033$ and $P = 0.001$ from

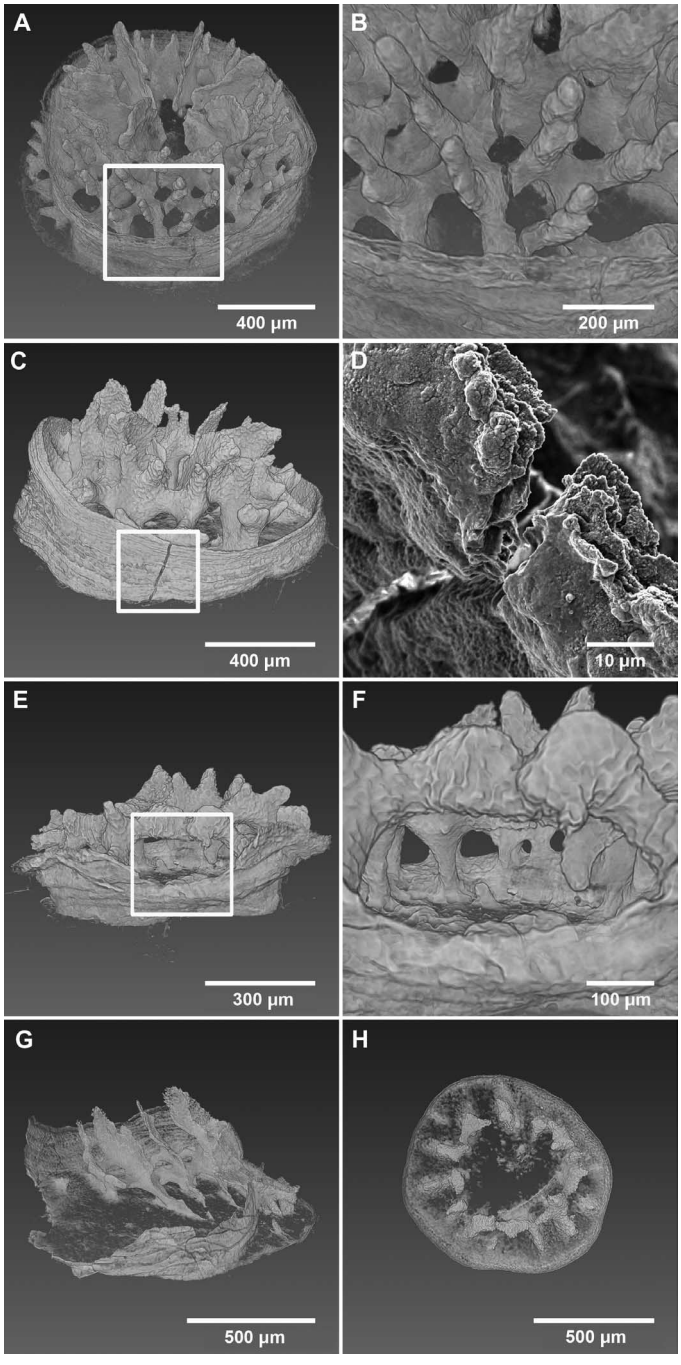

Fig. 2. Fractures and deformed skeletal structures in high Pco_2–treated corals. Fractures in the septa (**A** and **B**) and corallite wall (**C** and **D**). Small sections of missing septa and synapticulae (**E** and **F**). Gross deformities, with large sections of the skeleton missing or malformed (**G** and **H**).

Bonferroni pairwise comparisons between high PCO_2 and high T + PCO_2 for height and tertiary septa length-to-width ratios, respectively; Fig. 3 and table S2). Elevated temperature appeared to somewhat mitigate the negative effects of high PCO_2 on skeletal growth, particularly appearing to facilitate vertical growth at high PCO_2. Although there were no significant differences in corallite wall thickness between treatments, the eroded and highly porous surfaces of high-PCO_2 corals at both temperatures demonstrate that the microstructure of the corallite wall was severely altered by high PCO_2, even if the larger scale structure of the wall was not.

DISCUSSION

Our results indicate that coral recruits are unable to build normal calcium carbonate skeletons under high PCO_2 and low pH conditions. High PCO_2 resulted in structurally compromised skeletons that were smaller (increased SA/vol, reduced diameter and height), more fragile (thinner basal plate, pitted or porous corallite walls), and asymmetric. A higher frequency of fractures was also observed in the high-PCO_2 corals. Although the formation of these was likely an artifact of sample handling and processing after the experiment, it is remarkable that 50% of the individuals grown under acidified conditions had skeletal fractures, whereas no fractures were observed in skeletons grown under low PCO_2 conditions. Alternatively, the fractures may have occurred during the experiment while the recruits were still alive and growing their skeletons. Perhaps the increased porosity and reduced structural thickness caused fractures to form in situ under the mechanical strains of an actively growing skeleton. Future studies will need to examine this possibility with greater scrutiny. Consistent with the SEM data, fractures recorded in the high-PCO_2 environment highlight a more fragile, porous skeleton. A recent study on adult corals similarly reports that acidification causes more porous skeletal structures, but at a much higher PCO_2 than that applied to the juvenile corals studied here (PCO_2 ~ 2200 and 3800 versus 900 µatm) (*25*). Our results highlight how acutely vulnerable the growth and development of juvenile corals are to the changes in ocean chemistry expected to occur over the coming century under a business-as-usual scenario (RCP 8.5) (*1*, *26*). Although our low PCO_2 conditions were lower than present-day ambient conditions (~250 versus 390 µatm), it is unlikely that this lower PCO_2 condition influenced the overall conclusions of this study given that (i) the impacts of the high PCO_2 treatment on the skeleton were so severe, (ii) the difference in PCO_2 between present-day and the low PCO_2 treatments (~140 µatm) is much smaller than the difference between the low and high PCO_2 treatments (~650 µatm), and (iii) research comparing juvenile calcification under preindustrial and current ambient conditions has shown no significant differences (*27*). Nonetheless, it is possible that the more preindustrial PCO_2 levels used in our controls could have led to greater differences in skeletal deposition between the low and high PCO_2 conditions.

Corals are not the only calcifiers that experience deformation of their skeletal structure under acidified conditions. Skeletal asymmetry and microstructural abnormalities have been observed in both sea urchin juveniles and brittle star larvae exposed to acidified conditions (*28*–*31*). One study suggested that acidification might affect brittle star larval symmetry through the symmetry-controlling ion-flux mechanism (*29*, *32*). This mechanism induces left-right symmetry breakage in sea urchin larvae through asymmetrically localized control of H^+ and K^+ transport (*32*). It is possible that similar mechanisms are responsible for the CO_2-driven skeletal asymmetry observed in the coral recruits studied here. In addition, features indicative of mineral dissolution (that is, disorganized aragonite bundles and an overall pitted appearance of the skeletal surface) have also been observed in adult corals exposed to acidified conditions at natural CO_2 vents (*12*). However,

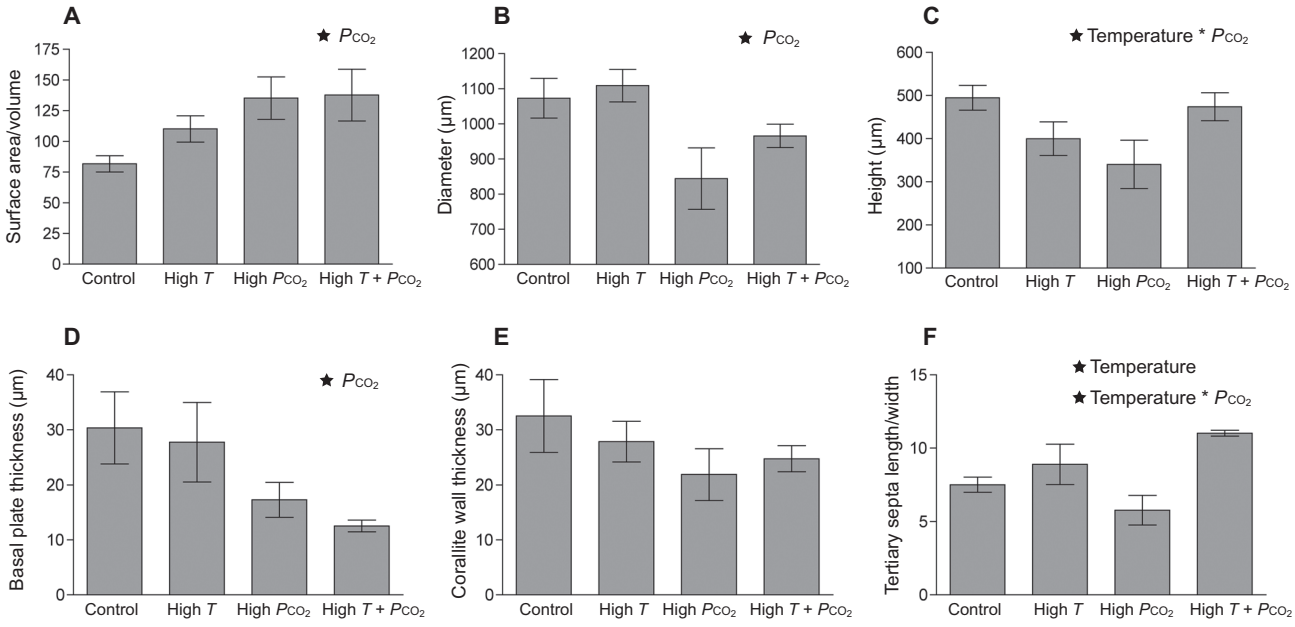

Fig. 3. Quantitative output from x-ray microscopy scans of 1-month-old coral skeletons under the four temperature-P_{CO_2} treatments (mean ± SE). (**A** to **F**) Measurements include (A) SA/vol ratio, (B) diameter, (C) height, (D) basal plate thickness, (E) corallite wall thickness, and (F) tertiary septa length/width ratio. Factors [temperature, P_{CO_2}, or their interaction (temperature *P_{CO_2})] significantly contributing to differences between treatments are indicated by ★ at the top of the graph (n = 5 individuals per treatment). See table S2 for details on statistical tests.

disordered crystals were only observed in areas of exposed skeleton (that is, parts of the skeleton not covered by tissue), whereas areas where a tissue layer covered the whole skeleton exhibited no such dissolution characteristics (*12*). The skeletons of juvenile corals in our study were completely covered in a tissue layer throughout the experiment and yet still showed deep pitting on the skeletal surface, which could indicate dissolution. This may be due to juveniles having a much thinner tissue layer for protection (*33*) compared to adult corals and further highlights the vulnerability of juvenile skeletogenesis under elevated P_{CO_2}.

As some coral reefs currently experience elevated P_{CO_2} (and suppressed pH) relative to the open ocean (up to ~500 µatm) (*34*, *35*), it is possible that recruits are adopting mechanisms to cope with these conditions in situ. A recent study has shown that adult corals living in highly dynamic thermal and chemical environments more rigorously control the up-regulation of pH within the calcifying fluid, thus demonstrating a greater resilience to the effects of ocean acidification (*36*). Whether or not coral recruits that have spawned from or settled in such highly variable reef environments also exhibit a greater degree of physiological resilience to acidification remains to be seen. Alternatively, new recruits may already be calcifying at reduced rates (relative to preindustrial conditions) in these environments. The reduced ability to quickly produce a robust skeleton in new coral recruits can have a direct impact on survival rates. For example, reduced growth rates in 2-month-old coral recruits, under elevated P_{CO_2}, led to reductions in overall survivorship due to elevated predation mortality, demonstrating how size-escape thresholds can shift under ocean acidification (*37*). However, it is important to recognize that those individuals that do survive the smaller and more susceptible size classes may be better able to cope with high P_{CO_2} conditions than (i) prior generations and (ii) as they get larger, which may offset the more severe effects on the skeleton in the early post-recruitment stages.

In contrast to the effects of acidification, our results suggest that the initial effects of ocean warming (+3°C) on calcification in subtropical juveniles could either be minimal or may even help to mitigate the negative impacts of elevated P_{CO_2}; however, whether the same response is seen in other subtropical species is yet to be tested. This result is contrary to studies that have been carried out in the tropics, where high temperature has exacerbated reductions in calcification under high P_{CO_2}, in both juvenile (*24*) and adult (*2*, *12*) corals. Tropical corals exist close to their upper thermal limit (*38*) and yet are presumably growing within the optimal range of temperatures for calcification. Consequently, a 3°C increase in temperature could subject them to thermal stress and depress calcification rates below optimal levels. In contrast, subtropical coral larvae and new recruits appear to withstand moderate (+3°C) increases in temperature (*23*, *39*). This may be a result of subtropical corals being acclimated to the wider annual range of temperatures generally experienced at higher-latitude locations. Additionally, the ability of new recruits to withstand moderate temperature increases could be related to larval dispersal in the water column, where larvae must survive, often for extended periods, over long distances, and through changing thermal environments (*23*, *40*, *41*).

In conclusion, acidified conditions caused severely abnormal skeletogenesis in new coral recruits. Although the partially mitigative effect of elevated temperature is encouraging in these subtropical recruits, taller but similarly fragile skeletons may not provide and sustain the structural support and protection required during early post-recruitment. Furthermore, this mitigative effect does not appear to be present in tropical coral recruits (*24*). Our data show that new recruits are thus highly vulnerable to acidification and indicate that near-future projections for ocean carbonate chemistry (*1*, *26*) have the potential to heavily reduce

post-recruitment success. Disruptions to normal skeletal development in new recruits could compromise the ability of coral reefs to successfully migrate to more suitable thermal environments, as well as inhibit the replenishment of existing reefs after episodic disturbances caused by storms, disease outbreaks, and mass bleaching events—all of which are expected to increase over the next century if the present CO_2 trajectory is not abated.

MATERIALS AND METHODS

Collection methods

Gravid adult colonies of the abundant plate coral species *A. spicifera* were collected off Basile Island in the Pelsaert group of the Houtman Abrolhos Islands (28°52′S, 113°57′E) in Western Australia, before the 2013 March mass-spawning event. Colonies were maintained in flow-through outdoor aquaria exposed to natural lighting, which received seawater filtered through a 20-μm nylon mesh. On the night of spawning, fertilized eggs (cross-fertilized from six spawning colonies, representing equal contributions from all six genotypes) were transferred to larval rearing tanks and maintained under ambient conditions until the larvae reached the planulae stage of development at 6 days post fertilization. Larvae were then transferred to treatment tanks (four replicate tanks per treatment).

Experimental design

All seawater entering the aquarium system was foam-fractionated and ultraviolet-sterilized to remove solids and bacteria. Seawater was treated in four separate sump tanks (one sump per treatment) that flowed into the replicate tanks every 3 hours for an ~90% water change. The carbonate chemistry was adjusted using a pH-dependent feedback system, which bubbled pure CO_2 into the seawater when pH deviated 0.01 pH units from set values (CO_2 Set Professional, AquaMedic). The pH was checked manually in all tanks every second day. The pH was measured on the total scale (±0.03) using a Schott Handylab pH meter equipped with a Blueline 24 electrode and calibrated against a combination of NBS (pH 4 and 7) and artificial seawater (tris) buffers; the latter was calibrated against certified reference materials (CRMs), provided by A. Dickson at the Scripps Institute of Oceanography (batch #7). Total Alkalinity (TA, ±5 μmol/kg) samples were taken once a week and measured using a single end-point titration to a spectrophotmetrically determined pH of ~4.0 (*42*), and calibrated against CRMs, also provided by A. Dickson (batch #105). Salinity was checked twice a week using a refractometer (35.5). Aragonite saturation state (Ω_{ar}) and P_{CO_2} were calculated from pH, TA, salinity, and temperature using the program CO2SYS (*43*). Water temperature was controlled with heater chillers (Resun, CL 150) and monitored using Hobo Pendant temperature loggers (±0.5° to ±0.9°C). The four temperature-P_{CO_2} conditions are outlined in table S1. The annual temperature range at the Abrolhos is ~19° to 24°C (*44*). Thus, the high-temperature treatment (27°C) represents an elevation of 3°C above the maximum monthly mean water temperature at the Abrolhos, which occurs around spawning time (24°C). The high P_{CO_2} treatment (P_{CO_2} ~ 900 μatm) is similar to projections for the year 2100 under the RCP 8.5 scenario (~930 μatm) (*26*). The low P_{CO_2} treatments are closer to preindustrial (250 μatm) than present-day atmospheric levels (~390 μatm). This was likely due to seawater being pumped into the experimental facility in the afternoon when photosynthesis of benthic primary producers in the region was driving P_{CO_2} below atmospheric levels. A rigorous study of the variation in carbonate chemistry at the Abrolhos is yet to be undertaken; however, spot measurements taken over 2011 to 2013 show the range for P_{CO_2} and pH to be ~300 to 500 μatm and ~7.9 to 8.1, respectively (*45*). Light levels were maintained at a 12:12–hour light/dark cycle, with a mean (±SE) light intensity of 212 ± 8 μmol photons m^{-2} s^{-1} (Biospherical Instruments, QSL-2100). The light levels applied in this (212 μmol photons m^{-2} s^{-1}) and other juvenile calcification studies (62 to 135 μmol photons m^{-2} s^{-1}) (*20–22*, *24*, *27*) are relatively low compared to the natural light levels experienced on a shallow reef. Higher light intensities experienced in situ may increase calcification relative to those recorded in laboratory experiments; however, larvae often show a preference during settlement for microcrevices and ledges that offer protection from predators but are presumably exposed to lower light intensities. Thus, the lower light levels we used may be more representative of their environment in the early post-recruitment phase.

Larval settlement

Larvae (n = 40) were transferred into 50-ml clear acrylic tubes, with a 100-μm mesh at the ends to allow water exchange. Plastic transparency paper, washed and soaked in ambient seawater for 1 week, lined the inside of the tubes. The transparency paper lining was used both for easy removal of the recruit skeletons at the end of the experiment and as a low-density substrate, easily excluded from 3D x-ray microscopy measurements of the skeleton. Three small (0.5 cm^2) crustose coralline algae chips (*Hydrolithon*), collected from the same site as the adult *A. spicifera* colonies, were added to each tube to induce settlement. Twelve tubes were transferred into each replicate treatment tank. Because of logistical constraints, each tank housed multiple larval tubes, resulting in a partial pseudoreplicate design (independent tanks with replicated tubes). Although the larvae had no measureable impact on the environmental conditions in each treatment, skeletal analyses were performed on individuals randomly selected across tubes and tanks to help counter pseudoreplication within the experimental design. At 7 days post settlement, recruits were inoculated with cultured clade C1 zooxanthellae (V. Beltran, AIMS), a common clade in this region (*46*). Settled juveniles were grown for 4 weeks post settlement under treatment conditions. Before termination of the experiment, each individual was examined and photographed using both a stereoscope and a fluorescence microscope to verify that the recruits were alive until the endpoint of the experiment. To remove organic material, the recruits were immersed in 3 to 7% sodium hypochlorite and rinsed three times in deionized water.

X-ray microscopy settings

Five primary polyps were randomly selected across tubes and tanks from each treatment for x-ray microscopy analyses. Randomly selected recruits also needed to meet four selection criteria to be usable for scanning: (i) were in the primary polyp stage of development, (ii) had settled on the plastic transparency paper, (iii) had settled a suitable distance from other recruits, and (iv) had remained attached to the paper and undamaged throughout processing. All x-ray scans were conducted using an Xradia Versa XRM520 x-ray microscope. Scanning was undertaken under the following conditions to produce data with ~1.3-μm pixel resolution: voltage, 50 kV; power, 4 W; exposure time, 20 s; binning, 2; and angle, full 360°, with a total of 3201 projections per sample. Reconstruction of the projections was conducted using the Xradia software XMReconstructor. Because of the long scan times

associated with obtaining high-resolution 3D images (~19 hours per individual recruit), only five individuals per treatment were scanned. However, the small variation within each treatment in the quantitative output indicated that this replication was sufficient.

Quantitative data extraction

The software Avizo Fire was used to process the reconstructed projections and extract quantitative data. The Edit New Label Field tool was used to set threshold radiodensity values, which removed the transparency paper, leaving only the $CaCO_3$ skeleton. The samples were then volume-rendered to create a 3D image. A label analysis was conducted on the segmented data set to determine the surface area and volume of the sample. All other measurements were made manually, using the Measure tool (fig. S4). For height, corallite wall thickness, and basal plate thickness, the mean of three measurements per sample was determined, whereas the mean diameter was calculated from four measurements per sample. For height and basal plate thickness, the three highest or thickest points in the sample were selected by scrolling through the slices of the sample. For diameter and corallite wall thickness, a single slice near the base showing the whole diameter was selected, and measurements were taken at the same points and along the same axis for each sample. The length and width were measured for all tertiary septa.

Correlative SEM

After x-ray scanning, the same individuals were mounted on stubs with carbon tabs while still attached to the transparency paper. The sample was surrounded with carbon tape, and the whole tab was then coated with 10 nm of platinum and 10 nm of carbon. Images from the top of the corallite wall and the tips of the tertiary septa were acquired at 5 kV using a Zeiss 55 field emission scanning electron microscope. The two areas of interest were selected on the basis of their rough or porous appearance in the 3D reconstructions of high-P_{CO_2} skeletons.

Statistical analysis

Two-way analyses of variance were conducted on the x-ray microscopy measurements to test for significant effects of elevated temperature, P_{CO_2}, and their interaction (table S2). All data were checked for equality of variance with Levene's test for homogeneity. The Shapiro-Wilk test was used to check for normality, and data were log-transformed if normality assumptions were not met. Bonferroni post hoc analyses were conducted when statistically significant interactive effects were found. All statistical analyses were conducted in SPSS version 21. The software PRIMER 7 was used to carry out sample ordination to better visualize how the recruits separate from each other. Similarity in each of the measurements was calculated using Bray-Curtis similarity coefficients of the data sets and then plotted using nonmetric multidimensional scaling (nMDS). nMDS plots were constructed for each measurement individually (fig. S9) and for all of the measurements together (fig. S10).

SUPPLEMENTARY MATERIALS

Supplementary material for this article is available at http://advances.sciencemag.org/cgi/content/full/2/2/e1501130/DC1

Fig. S1. Variation in seawater pH (A), total alkalinity (B), P_{CO_2} (C), and aragonite saturation state (D) in each treatment for the duration of the experiment.

Fig. S2. Variation in pH with time of day for each treatment.

Fig. S3. Top-down and side-view 3D x-ray images identifying the key skeletal structures discussed in this study.

Fig. S4. Examples of manual measurements of diameter, corallite wall thickness (A and B), tertiary septa length/width ratio (C and D), and height and basal plate thickness (E and F).

Fig. S5. All remaining individuals from the control (that is, excluding the individual shown in Fig. 1).

Fig. S6. All remaining individuals from the high *T* treatment (that is, excluding the individual shown in Fig. 1).

Fig. S7. All remaining individuals from the high P_{CO_2} treatment (that is, excluding the individual shown in Fig. 1).

Fig. S8. All remaining individuals from the high T + P_{CO_2} treatment (that is, excluding the individual shown in Fig. 1).

Fig. S9. nMDS ordination in two dimensions of quantitative output from 3D x-ray microscopy scans of juvenile coral skeletons, including SA/vol (A), diameter (B), height (C), basal plate thickness (D), corallite wall thickness (E), and tertiary septa length/width ratio (F) for individuals grown under different temperature-P_{CO_2} regimes.

Fig. S10. nMDS ordination in two dimensions, pooling all measures from 3D x-ray microscopy scans of juvenile coral skeletons.

Table S1. Physical and chemical conditions maintained in each treatment for the duration of the experiment [mean ± SD; Foster *et al.* (*23*)].

Table S2. Two-way ANOVAs testing for significant effects of temperature, P_{CO_2}, and interactions between the two factors (temperature * P_{CO_2}) on x-ray microscopy measurements of juvenile coral skeletons.

Movie S1. Skeleton of a 1-month-old coral recruit grown under control (24°C and 250 μatm) conditions.

Movie S2. Skeleton of a 1-month-old coral recruit grown under high P_{CO_2} (24°C and 900 μatm) conditions.

REFERENCES AND NOTES

1. IPCC, *Climate Change 2013: The Physical Science Basis. An Overview of the Working Group 1 Contribution to the Fifth Assessment Report of the Intergovernmental Panel on Climate Change (IPCC)* (Cambridge Univ. Press, New York, 2013).
2. S. Reynaud, N. Leclercq, S. Romaine-Lioud, C. Ferrier-Pagés, J. Jaubert, J.-P. Gattuso, Interacting effects of CO_2 partial pressure and temperature on photosynthesis and calcification in a scleractinian coral. *Glob. Chang. Biol.* **9**, 1660–1668 (2003).
3. G. Déath, J. M. Lough, K. E. Fabricius, Declining coral calcification on the Great Barrier Reef. *Science* **323**, 116–119 (2009).
4. D. P. Manzello, Coral growth with thermal stress and ocean acidification: Lessons from the eastern tropical Pacific. *Coral Reefs* **29**, 749–758 (2010).
5. P. L. Jokiel, S. L. Coles, Effects of temperature on the mortality and growth of Hawaiian reef corals. *Mar. Biol.* **43**, 201–208 (1977).
6. A. T. Marshall, P. Clode, Calcification rate and the effect of temperature in a zooxanthellate and an azooxanthellate scleractinian reef coral. *Coral Reefs* **23**, 218–224 (2004).
7. C. Langdon, T. Takahashi, C. Sweeney, D. Chipman, J. Goddard, F. Marubini, H. Aceves, H. Barnett, M. J. Atkinson, Effect of calcium carbonate saturation state on the calcification rate of an experimental coral reef. *Global Biogeochem. Cy.* **14**, 639–654 (2000).
8. F. Marubini, H. Barnett, C. Langdon, M. J. Atkinson, Dependence of calcification on light and carbonate ion concentration for the hermatypic coral *Porites compressa*. *Mar. Ecol. Prog. Ser.* **220**, 153–162 (2001).
9. C. Langdon, M. J. Atkinson, Effect of elevated pCO_2 on photosynthesis and calcification of corals and interactions with seasonal change in temperature/irradiance and nutrient enrichment. *J. Geophys. Res. Oceans* **110**, 1–16 (2005).
10. N. Muehllehner, P. J. Edmunds, Effects of ocean acidification and increased temperature on skeletal growth of two scleractinian corals, *Pocillopora meandrina* and *Porites rus*, *Proceedings of the 11th International Coral Reef Symposium*, 7 to 11 July 2008, Ft. Lauderdale, Florida.
11. V. Schoepf, A. G. Grottoli, M. E. Warner, W.-J. Cai, T. F. Melman, K. D. Hoadley, D. T. Pettay, X. Hu, Q. Li, H. Xu, Y. Wang, Y. Matsui, J. H. Baumann, Coral energy reserves and calcification in a high-CO_2 world at two temperatures. *PLOS One* **8**, e75049 (2013).
12. R. Rodolfo-Metalpa, F. Houlbrèque, É. Tambutté, F. Boisson, C. Baggini, F. P. Patti, R. Jeffree, M. Fine, A. Foggo, J.-P. Gattuso, J. M. Hall-Spencer, Coral and mollusc resistance to ocean acidification adversely affected by warming. *Nat. Clim. Chang.* **1**, 308–312 (2011).
13. R. Albright, B. Mason, C. Langdon, Effect of aragonite saturation state on settlement and post-settlement growth of *Porites astreoides* larvae. *Coral Reefs* **27**, 485–490 (2008).
14. R. Albright, B. Mason, M. Miller, C. Langdon, Ocean acidification compromises recruitment success of the threatened Caribbean coral *Acropora palmata*. *Proc. Natl. Acad. Sci. U.S.A.* **107**, 20400–20404 (2010).
15. R. Albright, C. Langdon, Ocean acidification impacts multiple early life history processes of the Caribbean coral *Porites astreoides*. *Glob. Chang. Biol.* **17**, 2478–2487 (2011).
16. A. P. Negri, P. A. Marshall, A. J. Heyward, Differing effects of thermal stress on coral fertilization and early embryogenesis in four Indo Pacific species. *Coral Reefs* **26**, 759–763 (2007).

17. P. Edmunds, R. Gates, D. Gleason, The biology of larvae from the reef coral *Porites astreoides*, and their response to temperature disturbances. *Mar. Biol.* **139**, 981–989 (2001).
18. N. S. Webster, S. Uthicke, E. S. Botté, F. Flores, A. P. Negri, Ocean acidification reduces induction of coral settlement by crustose coralline algae. *Glob. Chang. Biol.* **19**, 303–315 (2013).
19. R. H. Richmond, Reproduction and recruitment in corals: Critical links in the persistence of reefs, in *Life and Death of Coral Reefs*, C. Birkeland, Ed. (Chapman & Hall, New York, 1997), pp. 175–197.
20. A. L. Cohen, D. C. McCorkle, S. de Putron, G. A. Gaetani, K. A. Rose, Morphological and compositional changes in the skeletons of new coral recruits reared in acidified seawater: Insights into the biomineralization response to ocean acidification. *Geochem. Geophys. Geosys.* **10**, 1–12 (2009).
21. S. J. de Putron, D. C. McCorkle, A. L. Cohen, A. B. Dillon, The impact of seawater saturation state and bicarbonate ion concentration on calcification by new recruits of two Atlantic corals. *Coral Reefs* **30**, 321–328 (2011).
22. E. J. Drenkard, A. L. Cohen, D. C. McCorkle, S. J. de Putron, V. R. Starczak, A. E. Zicht, Calcification by juvenile corals under heterotrophy and elevated CO_2. *Coral Reefs* **32**, 727–735 (2013).
23. T. Foster, J. P. Gilmour, C. M. Chua, J. L. Falter, M. T. McCulloch, Effect of ocean warming and acidification on the early life stages of subtropical *Acropora spicifera*. *Coral Reefs* **34**, 1217–1226 (2015).
24. H. Anlauf, L. D'Croz, A. O'Dea, A corrosive concoction: The combined effects of ocean warming and acidification on the early growth of a stony coral are multiplicative. *J. Exp. Mar. Biol. Ecol.* **397**, 13–20 (2011).
25. E. Tambutté, A. A. Venn, M. Holcomb, N. Segonds, N. Techer, D. Zoccola, D. Allemand, S. Tambutté, Morphological plasticity of the coral skeleton under CO_2-driven seawater acidification. *Nat. Commun.* **6**, 7368 (2015).
26. M. Meinshausen, S. J. Smith, K. Calvin, J. S. Daniel, M. L. T. Kainuma, J.-F. Lamarque, K. Matsumoto, S. A. Montzka, S. C. B. Raper, K. Riahi, A. Thomson, G. J. M. Velders, D. P. P. van Vuuren, The RCP greenhouse gas concentrations and their extensions from 1765 to 2300. *Clim. Change* **109**, 213–241 (2011).
27. S. Ohki, T. Irie, M. Inoue, K. Shinmen, H. Kawahata, T. Nakamura, A. Kato, Y. Nojiri, A. Suzuki, K. Sakai, R. van Woesik, Calcification responses of symbiotic and aposymbiotic corals to near-future levels of ocean acidification. *Biogeosciences* **10**, 6807–6814 (2013).
28. M. Byrne, M. Ho, E. Wong, N. A. Soars, P. Selvakumaraswamy, H. Sheppard-Brennand, S. A. Dworjanyn, A. R. Davis, Unshelled abalone and corrupted urchins: Development of marine calcifiers in a changing ocean. *Proc. Biol. Sci.* **278**, 2376–2383 (2011).
29. S. Dupont, J. Havenhand, W. Thorndyke, L. Peck, M. Thorndyke, Near-future level of CO_2-driven ocean acidification radically affects larval survival and development in the brittlestar *Ophiothrix fragilis*. *Mar. Ecol. Prog. Ser.* **373**, 285–294 (2008).
30. H. Kurihara, A. Shirayama, Effects of increased atmospheric CO_2 on sea urchin early development. *Mar. Ecol. Prog. Ser.* **274**, 161–169 (2004).
31. H. Sheppard-Brennand, N. Soars, S. A. Dworjanyn, A. R. Davis, M. Byrne, R. K. F. Unsworth, Impact of ocean warming and ocean acidification on larval development and calcification in the sea urchin *Tripneustes gratilla*. *PLOS One* **5**, e11372 (2010).
32. T. Hibino, Y. Ishii, M. Levin, A. Nishino, Ion flow regulates left–right asymmetry in sea urchin development. *Dev. Genes Evol.* **216**, 265–276 (2006).
33. S. V. Vollmer, P. J. Edmunds, Allometric scaling in small colonies of the scleractinian coral *Siderastrea siderea* (Ellis and Solander). *Biol. Bull.* **199**, 21–28 (2000).
34. R. Albright, C. Langdon, K. R. N. Anthony, Dynamics of seawater carbonate chemistry, production, and calcification of a coral reef flat, central Great Barrier Reef. *Biogeosciences* **10**, 6747–6758 (2013).
35. A. Sutton, D. Manzello, B. Gintert, Coupling chemical and biological monitoring to understand the impact of ocean acidification on coral reef ecosystems. *Oceanography* **28**, 28–29 (2015).
36. L. Georgiou, J. Falter, J. Trotter, D. I. Kline, M. Holcomb, S. G. Dove, O. Hoegh-Guldberg, M. McCulloch, pH homeostasis during coral calcification in a free ocean CO_2 enrichment (FOCE) experiment, Heron Island reef flat, Great Barrier Reef. *Proc. Natl. Acad. Sci. U.S.A.* **112**, 13219–13224 (2015).
37. C. Doropoulos, S. Ward, A. Marshell, G. Diaz-Pulido, P. J. Mumby, Interactions among chronic and acute impacts on coral recruits: The importance of size-escape thresholds. *Ecology* **93**, 2131–2138 (2012).
38. R. Berkelmans, B. L. Willis, Seasonal and local spatial patterns in the upper thermal limits of corals on the inshore Central Great Barrier Reef. *Coral Reefs* **18**, 219–228 (1999).
39. Y. Nozawa, P. L. Harrison, Effects of elevated temperature on larval settlement and post-settlement survival in scleractinian corals, *Acropora solitaryensis* and *Favites chinensis*. *Mar. Biol.* **152**, 1181–1185 (2007).
40. E. A. Treml, P. N. Halpin, D. L. Urban, L. F. Pratson, Modeling population connectivity by ocean currents, a graph-theoretic approach for marine conservation. *Landscape Ecol.* **23**, 19–36 (2008).
41. H. M. Putnam, P. J. Edmunds, T.-Y. Fan, Effect of a fluctuating thermal regime on adult and larval reef corals. *Invertebr. Biol.* **129**, 199–209 (2010).
42. W. Yao, R. H. Byrne, Simplified seawater alkalinity analysis: Use of linear array spectrometers. *Deep Sea Res. Pt. I* **45**, 1383–1392 (1998).
43. E. Lewis, D. Wallace, L. J. Allison, *Program Developed for CO_2 System Calculations* (Carbon Dioxide Information Analysis Center, Oak Ridge National Laboratory, U.S. Department of Energy, Oak Ridge, TN, 1998).
44. A. Pearce, M. Rossbach, M. Tait, R. Brown, *Sea Temperature Variability Off Western Australia 1990 to 1994* (Department of Fisheries, Western Australia, 1999), vol. **111**, pp. 1–45.
45. T. Foster, J. A. Short, J. L. Falter, C. Ross, M. T. McCulloch, Reduced calcification in Western Australian corals during anomalously high summer water temperatures. *J. Exp. Mar. Biol. Ecol.* **461**, 133–143 (2014).
46. R. N. Silverstein, A. Correa, T. C. LaJeunesse, A. C. Baker, Novel algal symbiont (*Symbiodinium* spp.) diversity in reef corals of Western Australia. *Mar. Ecol. Prog. Ser.* **422**, 63–75 (2011).

Acknowledgments: We thank the Batavia Coast Maritime Institute and the Centre for Microscopy, Characterisation and Analysis (UWA) for technical assistance and access to facilities. We thank the Basile family for logistical and technical support at the Abrolhos Islands. Many thanks to the people who donated their time and resources to this project, including L. Foster, T. Foster, A. Basile, T. Basile, P. Scarpuzza, J. Melvin, C. Wood, M. Chua, K. Antipas, Z. Snedden, A. Mitchell, M. van Keulen, V. Beltran, and J. Shaw. **Funding:** This research was supported by the ARC Centre of Excellence for Coral Reef Studies (CE0561435) and ARC Laureate Funding to M.T.M. (FL120100049). **Author contributions:** T.F. designed the experiment with P.L.C., M.T.M., and J.L.F.; T.F. conducted the experiment; T.F. and P.L.C. conducted x-ray and SEM work; T.F. analyzed the data and wrote the paper; P.L.C., M.T.M., and J.L.F. read and commented on the manuscript. **Competing interests:** The authors declare that they have no competing interests. **Data and materials availability:** All data needed to evaluate the conclusions in the paper are present in the paper and/or the Supplementary Materials. CRMs available by request from the Marine Physical Laboratory at Scripps. Additional data related to this paper may be requested from the authors.

Submitted 19 August 2015
Accepted 7 December 2015
Published 19 February 2016
10.1126/sciadv.1501130

Citation: T. Foster, J. L. Falter, M. T. McCulloch, P. L. Clode, Ocean acidification causes structural deformities in juvenile coral skeletons. *Sci. Adv.* **2**, e1501130 (2016).

Ocean acidification causes structural deformities in juvenile coral skeletons

Taryn Foster, James L. Falter, Malcolm T. McCulloch and Peta L. Clode

Sci Adv **2** (2), e1501130.
DOI: 10.1126/sciadv.1501130